Video Article

Preparation of Carbon Nanosheets at Room Temperature

Stephen Schrettl[1], Bjoern Schulte[1], Cristina Stefaniu[2], Joana Oliveira[2], Gerald Brezesinski[2], Holger Frauenrath[1]

[1]Institute of Materials, Ecole Polytechnique Fédérale de Lausanne (EPFL)

[2]Colloid Chemistry Department, Max Planck Institute of Colloids and Interfaces

Correspondence to: Holger Frauenrath at holger.frauenrath@epfl.ch

URL: https://www.jove.com/video/53505
DOI: doi:10.3791/53505

Keywords: Chemistry, Issue 109, oligoynes, amphiphiles, self-assembled monolayers, air-water interface, room temperature carbonization, nanosheets, carbon nanostructures

Date Published: 3/8/2016

Citation: Schrettl, S., Schulte, B., Stefaniu, C., Oliveira, J., Brezesinski, G., Frauenrath, H. Preparation of Carbon Nanosheets at Room Temperature. *J. Vis. Exp.* (109), e53505, doi:10.3791/53505 (2016).

Abstract

Amphiphilic molecules equipped with a reactive, carbon-rich "oligoyne" segment consisting of conjugated carbon-carbon triple bonds self-assemble into defined aggregates in aqueous media and at the air-water interface. In the aggregated state, the oligoynes can then be carbonized under mild conditions while preserving the morphology and the embedded chemical functionalization. This novel approach provides direct access to functionalized carbon nanomaterials. In this article, we present a synthetic approach that allows us to prepare hexayne carboxylate amphiphiles as carbon-rich siblings of typical fatty acid esters through a series of repeated bromination and Negishi-type cross-coupling reactions. The obtained compounds are designed to self-assemble into monolayers at the air-water interface, and we show how this can be achieved in a Langmuir trough. Thus, compression of the molecules at the air-water interface triggers the film formation and leads to a densely packed layer of the molecules. The complete carbonization of the films at the air-water interface is then accomplished by cross-linking of the hexayne layer at room temperature, using UV irradiation as a mild external stimulus. The changes in the layer during this process can be monitored with the help of infrared reflection-absorption spectroscopy and Brewster angle microscopy. Moreover, a transfer of the carbonized films onto solid substrates by the Langmuir-Blodgett technique has enabled us to prove that they were carbon nanosheets with lateral dimensions on the order of centimeters.

Video Link

The video component of this article can be found at https://www.jove.com/video/53505/

Introduction

Two-dimensional carbon nanostructures attract significant attention due to the reported outstanding electrical, thermal, as well as mechanical properties[1-5]. These materials are expected to further the technical progress in the fields of polymer composites[6], energy storage devices[7], and molecular electronics[8-10]. Despite intensive research efforts in recent years, however, access to larger amounts of well-defined carbon nanomaterials is still limited, which impedes their large-scale implementation in technological applications[11,12].

Carbon nanomaterials are accessible by either top-down or bottom-up approaches. Typical approaches such as exfoliation techniques[13] or high-energy processes on surfaces[14-16] offer the possibility to obtain materials with a high degree of structural perfection and very good performance. However, the isolation and purification of the products remains challenging, and the large-scale production of defined nanostructured materials is difficult[12]. On the other hand, bottom-up approaches can be employed that rely on the use of molecular precursors, their arrangement into defined structures, and a subsequent carbonization that yields the carbon nanostructures[17-23]. In this case, the precursors themselves are more complex and their preparation often requires multiple synthetic steps. These approaches may offer a high degree of control over the chemical and physical properties of the resulting materials and may furnish a direct access to tailored materials. However, the conversion of the precursors into carbon nanomaterials is typically performed at temperatures above 800 °C, which leads to a loss of the embedded chemical functionalization[24-27].

The above mentioned limitations have been addressed in our group by employing highly reactive oligoynes that can be converted into carbon nanomaterials at room temperature[28,29]. In particular, amphiphiles comprising a hydrophilic head group and a hexayne segment are accessible through a sequence of bromination and palladium-mediated Negishi cross-coupling reactions[30,31]. The conversion of these precursor molecules into the target structure occurs at or below room temperature upon irradiation with UV light. The high reactivity of the oligoyne amphiphiles makes the use of soft templates, such as the air-water interface or fluid-fluid interfaces, possible. In previous investigations, we successfully prepared vesicles from solutions of hexayne glycoside amphiphiles[28]. Cross-linking of these vesicles was achieved under mild conditions by UV irradiation of the samples. Moreover, we recently prepared self-assembled monolayers from hexaynes with a methyl carboxylate head group and a hydrophobic alkyl tail at the air-water interface in a Langmuir trough. The densely packed molecular precursors were then straightforwardly converted into self-supporting carbon nanosheets at room temperature by UV irradiation. In related approaches defined molecular precursors have recently been used for the preparation of two-dimensionally extended nanosheets at the air-water interface[32-38].

The aim of this work is to give a concise, practical overview of the overall synthesis and fabrication steps that allow for the preparation of carbon nanosheets from hexayne amphiphiles. The focus is on the experimental approach and preparative questions.

Protocol

Caution: Please make sure to consult the relevant materials safety data sheets (MSDS) before the use of any chemical compounds. Some of the chemicals used in these syntheses are acutely toxic and carcinogenic. Prepared nanomaterials may have additional hazards compared to their bulk counterpart. It is imperative to use all appropriate safety practices when performing reactions (fume hood) and personal protective equipment (safety glasses, gloves, lab coat, full length pants, closed-toe shoes). If not otherwise stated the following procedures involve standard Schlenk techniques[39].

1. Preparation of the Molecular Precursor[29,31]

1. Synthesis of 4-tritylphenyl 10(trimethylsilyl)deca-5,7,9-triynoate (1)
   Note: The required compounds for the subsequently described synthetic steps can be straightforwardly prepared following published literature procedures[29,31]. Thin layer chromatography (TLC) as well as column chromatography are carried out according to standard laboratory procedures[39,40].
   1. Dissolve 1,4-bistrimethylsilylbutadiene (7.82 g, 40.3 mmol) in dry tetrahydrofuran (THF, 50 ml) in an inert atmosphere in a Schlenk tube equipped with a septum. Stir the mixture and cool it to a temperature of 0 °C by immersion of the flask in an ice bath.
   2. Slowly add methyl lithium lithium bromide complex (17.9 ml, 2.2 M in Et_2O, 39.3 mmol) to this solution by syringe. Remove the cooling bath and allow the mixture to warm up to room temperature and leave stirring for 30 min.
   3. Immerse the Schlenk tube in an ice bath and cool the solution to a temperature of 0 °C. Slowly add a solution of zinc chloride (57.5 ml, 0.7 M in THF, 40.24 mmol) to the stirred solution. Remove the cooling bath, allow the solution to warm up to room temperature, and stir the mixture for additional 30 min.
   4. In a Schlenk flask, disperse the palladium catalyst $PdCl_2$(dppf) DCM (1.60 g, 1.96 mmol) in dry toluene (300 ml) in an inert atmosphere, and add 4-tritylphenyl 6-bromohex-5-ynoate (10.0 g, 19.63 mmol). Cool this mixture to a temperature of 0 °C by immersion of the Schlenk flask in an ice bath.
   5. Transfer the solution in the Schlenk tube containing the zinc acetylide to the Schlenk flask containing the bromoacetylene derivative and the palladium catalyst by employing a transfer cannula. Leave the mixture stirring and monitor the reaction by TLC[39]. Consider the reaction complete after TLC (DCM/*n*-heptane 2:1; coloring with *p*-anisaldehyde solution[39]) indicates that the bromoacetylene derivative (R_f: 0.64) is consumed (after approximately 16 hr).
   6. Dilute the reaction mixture with diethylether (Et_2O) (300 ml) and transfer it to a separatory funnel. Wash the organic phase three times with saturated ammonium chloride solution (300 ml) and once with saturated sodium chloride solution (300 ml).
   7. Transfer the organic phase from the separatory funnel to an Erlenmeyer flask and dry the organic phase over sodium sulfate (100 g). Remove the sodium sulfate by filtration and concentrate the organic phase *in vacuo*.
   8. Purify the crude product by column chromatography[40] (silica gel; dichloromethane/*n*-heptane 1:1) in order to obtain the desired product 1 (R_f: 0.33; 7.7 g, 71%) as a light brown solid. Check the purity of (1) by ^1H and $^{13}C\{^1H\}$ NMR spectroscopy[29].

2. Synthesis of 4-tritylphenyl octacosa-5,7,9,11,13,15-hexaynoate (2)
   Note: The synthesis of 4-tritylphenyl octacosa-5,7,9,11,13,15-hexaynoate 2 is carried out over two steps starting from 4-tritylphenyl 10(trimethylsilyl)deca-5,7,9-triynoate due to the observed low stability of the intermediate triyne bromide[41].
   1. Dissolve 4-tritylphenyl 10-(trimethylsilyl)deca-5,7,9-triynoate 1 (2.00 g, 3.63 mmol) in dry dichloromethane (DCM, 15 ml) in an inert atmosphere in a 100 ml Schlenk flask equipped with a septum. After dissolution of the compound, add dry acetonitrile (MeCN, 15 ml).
   2. Shield the Schlenk flask from light with aluminum foil and add *N*-bromosuccinimide (679 mg, 3.81 mmol) as well as silver fluoride (484 mg, 3.81 mmol). Stir the resulting mixture for 8 hr at room temperature and monitor the progress of the reaction by TLC. Consider the reaction complete after TLC (DCM/*n*-heptane 1:1; detection with *p*-anisaldehyde solution[39] as the coloring agent) indicates that the starting material (1) (R_f: 0.33) is consumed (after approximately 3 hr).
   3. Dilute the reaction mixture with DCM (30 ml) and transfer it into a separatory funnel. Wash the organic phase six times with a 1 M aqueous hydrogen chloride solution (60 ml) and once with a saturated aqueous sodium chloride solution (60 ml).
   4. Transfer the organic phase from the separatory funnel to an Erlenmeyer flask and dry the organic phase over sodium sulfate (50 g). Filter the organic phase and concentrate the filtrate *in vacuo* to approximately 10 ml, while thoroughly shielding it from light.
   5. Add dry toluene (20 ml) and concentrate the mixture once again *in vacuo* to a volume of approximately 5 ml.
   6. Dissolve 1-trimethylsilyloctadeca-1,3,5-triyne (2.28 g, 7.26 mmol) in dry THF (20 ml) in an inert atmosphere in a 100 ml Schlenk tube equipped with a rubber septum. Cool the solution to a temperature of 0 °C by immersion of the Schlenk tube in an ice bath.
   7. Slowly add methyl lithium lithium bromide complex (3.22 ml, 2.2 M in Et_2O, 7.08 mmol) and keep the temperature of the mixture at 0 °C for 45 min.
   8. To this mixture, slowly add a solution of zinc chloride (10.37 ml, 0.7 M in THF, 7.26 mmol). After the addition is completed, stir the resulting mixture for additional 45 min.
   9. In parallel, disperse the palladium catalyst $PdCl_2$(dppf) DCM (296 mg, 0.36 mmol) in dry toluene (100 ml) in an inert atmosphere in a 500 ml Schlenk flask equipped with a rubber septum. Cool the mixture to a temperature of 0 °C by immersion of the flask in an ice bath.
   10. Slowly add *n*-butyl lithium (0.29 ml, 2.5 M in *n*-hexane, 0.73 mmol) to the dispersion of the palladium catalyst in dry toluene. Remove the ice bath after complete addition, stir the mixture for 10 min at room temperature, and thereafter cool it to a temperature of 0 °C.
   11. Add the concentrated toluene solution containing the 4-tritylphenyl 10-bromodeca-5,7,9-triynoate (10 ml, 3.63 mmol) through a syringe simultaneously with the zinc acetylide solution (see above), which is added through a transfer cannula from the Schlenk tube. Shield the flask with the reaction mixture from light with aluminum foil.
   12. Monitor the progress of the reaction by TLC (DCM/*n*-heptane 1:1; detection with *p*-anisaldehyde solution[39] as the coloring agent). After complete consumption of 4-tritylphenyl 10-bromodeca-5,7,9 triynoate (R_f: 0.34; after approximately 48 hr), dilute the mixture with Et_2O

(100 ml) and transfer it into a separatory funnel. Wash the organic phase three times with a saturated aqueous ammonium chloride solution (200 ml) and once with a saturated aqueous sodium chloride solution (200 ml).
13. Transfer the organic phase to an Erlenmeyer flask and dry it over sodium sulfate (80 g). Filter the organic phase and concentrate the filtrate *in vacuo*.
14. Purify the crude product by column chromatography[40] (silica gel; DCM/*n*-heptane 1:1) to isolate 4-tritylphenyl octacosa-5,7,9,11,13,15-hexaynoate (2) (R_f: 0.43; 0.60 g, 23%) as a brown solid. Check the purity of (2) by ^{1}H and $^{13}C\{^{1}H\}$ NMR spectroscopy[29].

3. Synthesis of Methyl octacosa-5,7,9,11,13,15-hexaynoate (3)
    1. Dissolve 4-tritylphenyl octacosa-5,7,9,11,13,15-hexaynoate (2) (208 mg, 0.289 mmol) in DCM (15 ml) in an inert atmosphere in a 100 ml Schlenk flask, and add methanol (10 ml).
    2. Shield the flask from light with aluminum foil, and add sodium methanolate (31 mg, 0.578 mmol).
    3. Stir the resulting mixture for 30 min at room temperature. Thereafter, dilute with DCM (15 ml), transfer into a separatory funnel, wash once with a 1 M aqueous hydrogen chloride solution (30 ml), and once with saturated aqueous sodium chloride solution (30 ml).
    4. Transfer the organic phase into an Erlenmeyer flask and dry it over sodium sulfate (30 g). Filter the organic phase and concentrate the filtrate *in vacuo*.
    5. Purify the crude product by column chromatography[40] (silica gel; DCM/*n*-pentane 1:1) to isolate methyl octacosa-5,7,9,11,13,15-hexaynoate (3) (R_f: 0.62) as a yellow solution. Store the product of this reaction as a dilute DCM solution (10 ml) to minimize any decomposition.
    6. Transfer approximately 3 ml of the stock solution to a brown-glass round bottom flask and add $CDCl_3$ (5 ml). Concentrate the solution to approximately 1 ml *in vacuo*, add $CDCl_3$ (5 ml), and concentrate the solution to approximately 1 ml *in vacuo*. Perform ^{1}H and $^{13}C\{^{1}H\}$ NMR spectroscopy with this solution to check the purity of (3)[29].

4. Freeze-drying of the Methyl Ester and Preparation of a Stock Solution
    1. Prepare a stock solution of defined concentration (c = 1 mM) for experiments at the air-water interface. Transfer a fraction of the dilute solution of methyl octacosa-5,7,9,11,13,15-hexaynoate in DCM to a tared 50 ml brown-glass round bottom flask and concentrate the solution to approximately 1 ml *in vacuo*.
    2. Connect the flask to a vacuum line and immerse the flask in liquid nitrogen in order to freeze the concentrated solution. After the mixture has completely solidified, apply vacuum (approximately 5 x 10^{-3} mbar) to the flask and remove the flask from the liquid nitrogen.
    3. After complete removal of the residual solvent, weigh the flask while shielding it from light. Prepare a stock solution of defined concentration c = 1 mM by addition of the appropriate amount of chloroform. Shield the stock solution from light and store it at a temperature of -15 °C.

2. Film Formation of the Hexayne Amphiphile at the Air-water Interface

Note: All experiments at the air-water interface are carried out with computer-interfaced polytetrafluoroethylene Langmuir troughs with one (or two) barriers. The troughs are equipped with a surface pressure microbalance with a filter paper Wilhelmy plate. An external thermostat is used to maintain the temperature of the ultrapure water subphase at 20 °C. The Langmuir troughs are placed in a sealed box to avoid the contamination of the interface. Before measurements are carried out, the purity of the bare surface is checked by compression. All used experimental Langmuir setups are calibrated prior to use by employing a two-point calibration method: the bare water surface for 0 mN/m as well as the second-order transition from a tilted to a non-tilted state of stearic acid[42], that is not sensitive to temperature changes in the used temperature range. This ensures reliable and comparable measurements.

1. Measurement of the Surface Pressure-area Isotherm and Determination of the Compressibility Modulus
    1. Use a syringe to carefully spread 100 µl of the dilute stock solution of (3) in DCM/chloroform (c = 1 mmol/L) on the surface of the ultrapure water in a Langmuir trough.
    2. Leave the Langmuir trough to equilibrate for 15 min allowing the solvent to evaporate.
    3. Compress the layer with a constant compression rate of 5 Å/(molecule x min) by reducing the surface area of the Langmuir trough with the barriers. Simultaneously measure the surface pressure with the surface pressure microbalance equipped with a filter paper Wilhelmy plate. Continue the compression of the layer until a drop in the surface pressure indicates the collapse of the film.
    4. Repeat the surface pressure-area isotherm measurements as described in 2.1.1-2.1.3 two times with a clean Langmuir trough to ensure the reproducibility of the results.
    5. Determine the compressibility modulus from the isotherm of the layer according to the following relation[43]
    $C_s^{-1} = -A(\partial\Pi/\partial A)_T$
    where A is the mean molecular area and Π the surface pressure.

2. Investigation of the Stability of the Layer Below and Above the Plateau in the Isotherm
    1. Spread an aliquot of 100 µl of the dilute stock solution of (3) on ultrapure water in a Langmuir trough.
    2. Leave the Langmuir trough to equilibrate for 15 min allowing the solvent to evaporate.
    3. Compress the layer to a surface pressure of 8 mN/m with a constant compression rate of 5 Å/(molecule x min) by reducing the surface area of the Langmuir trough with the barriers. Continue the compression of the layer until the measured surface pressure reaches 8 mN/m and set the barriers so that this surface pressure is kept at a constant value.
    4. Monitor the development of the surface area as the barriers of the Langmuir trough adjust over the course of 45 min to maintain a constant surface pressure of 8 mN/m.
    5. Compress the layer to a surface pressure of 23 mN/m with a constant compression rate of 5 Å/(molecule x min) by further reducing the surface area of the Langmuir trough with the barriers. Set the barriers so that the surface pressure is kept constant at 23 mN/m.
    6. Monitor the development of the surface area as the barriers of the Langmuir trough adjust over the course of 45 min to maintain a constant surface pressure of 23 mN/m.

3. Characterization of the Layer by Infrared Reflection-absorption Spectroscopy
   Note: In order to record infrared (IR) spectra, an FT-IR spectrometer equipped with a liquid nitrogen-cooled mercury cadmium telluride (MCT) detector is employed and the latter is attached to an external air/water reflection unit. The IR beam is guided out of the spectrometer and focused onto the ultrapure water surface of the thermostated Langmuir trough. Light of *p*-polarization at an angle of incidence below (40°) the Brewster angle was used for the measurements. The Langmuir trough for IR measurements consists of two compartments: in one compartment, the sample monolayer system is spread, while the other compartment contains the ultrapure water subphase as a reference. A computer-controlled shuttle system is used to move the trough, so that either the sample or the reference compartment is illuminated. To eliminate the water vapor signal from the spectra, calculate the reflection-absorption spectrum according to $\log(R/R_0)$, with the single-beam reflectance spectrum from the reference compartment (R_0) as a background for the single-beam reflectance spectrum of the monolayer (R) from the sample compartment. Maintain the water vapor pressure constant by placing the whole experimental setup into a hermetically sealed box. In all experiments, use a resolution and scanner speed of 8 cm^{-1} and 20 kHz, respectively. Use a wire grid polarizer to polarize the incident IR beam. Co-add the spectra with *p*-polarized light over 400 scans. Perform a baseline-correction to allow for a comparison of the spectra.
   1. Spread an aliquot of 100 µl of the dilute stock solution of (3) on ultrapure water in a Langmuir trough comprising an infrared reflection-absorption (IRRA) spectroscopy setup.
   2. Leave the Langmuir trough to equilibrate for 15 min allowing the solvent to evaporate.
   3. Compress the layer to a surface pressure of 1 mN/m with a constant compression rate of 5 Å/(molecule x min) by reducing the surface area of the Langmuir trough with the barriers. Monitor the surface pressure by means of the surface pressure microbalance with a filter paper Wilhelmy plate and set the barriers of the Langmuir trough so that a surface pressure of 1 mN/m is maintained.
   4. Record an IR spectrum with *p*-polarized light at an angle of incidence of 40°[44,45].
   5. Compress the layer at a constant compression rate of 5 Å/(molecule x min) by further reducing the surface area of the Langmuir trough with the barriers so that surface pressures of 3, then 5, and finally 8 mN/m are obtained as indicated by the surface pressure microbalance. Record spectra with *p*-polarized light at an angle of incidence of 40° for each of these surface pressures while keeping the latter constant[44,45].

3. Carbonization of a Hexayne Amphiphile Monolayer at Room Temperature

Note: All experiments at the air-water interface are performed as described above. UV irradiation is carried out using a 250 W gallium-doped metal halide UV lamp (UV-Light Technology, Birmingham, United Kingdom). For carbonizations of films at the air-water interface, the box enclosing the Langmuir trough is carefully removed or opened at the side, and the lamp is placed 50 cm away from the water surface while ensuring that the air-water interface is covered in the cone of UV light. During illumination, the temperature of the subphase is maintained at 20 °C using the thermostat of the Langmuir trough. All carbonization experiments are performed at a surface pressure of 8 mN/m. At this pressure a tight packing of the amphiphiles is ensured while, at the same time, the monolayer displays a high stability.

1. Investigation of the Carbonization by IRRA Spectroscopy and Isotherm Measurement
   Note: IRRA spectra are recorded as described above[44,45].
   1. Spread an aliquot of 100 µl of the dilute stock solution of (3) on ultrapure water in the Langmuir trough comprising an infrared reflection-absorption spectroscopy (IRRA) setup.
   2. Leave the Langmuir trough to equilibrate for 15 min allowing the solvent to evaporate.
   3. Compress the layer at a constant compression rate of 5 Å/(molecule x min) by reducing the surface area of the Langmuir trough with the barriers so that a surface pressure of 8 mN/m is obtained as measured by the surface pressure microbalance equipped with a filter paper Wilhelmy plate. Set the barriers of the Langmuir trough so that a surface pressure of 8 mN/m is maintained.
   4. Record an IR spectrum with *p*-polarized light at an angle of incidence of 40°[44,45].
   5. Carefully remove the box enclosing the Langmuir trough. Mount the UV lamp to a support stand and place it approximately 50 cm away from the water surface while ensuring that the interface is covered in the cone of the UV light.
   6. After confirming that the monolayer is still compressed at a surface pressure of 8 mN/m as measured by the surface pressure microbalance, set the barriers of the Langmuir trough so that they are fixed at the current position.
   7. Expose the air-water interface to UV light. Stop the irradiation by turning the lamp off after a total of 40 min of irradiation. Monitor and record the change of the surface pressure by the surface pressure microbalance equipped with a filter paper Wilhelmy plate throughout the course of the irradiation.
   8. Enclose the Langmuir trough in the sealed box in order to avoid a contamination of the interface. Leave the setup to equilibrate for 30 min. Set the barriers of the Langmuir trough to maintain the surface pressure observed by the surface pressure microbalance after irradiation.
   9. Record an IR spectrum with *p*-polarized light at an angle of incidence of 40°[44,45].

2. Investigation of the Carbonized Film by Brewster Angle Microscopy
   Note: Brewster angle microscopy (BAM) experiments are performed on a custom-made computer-interfaced Langmuir trough coupled with a Brewster angle microscope as described elsewhere[46,47]. The surface pressure isotherms are continuously measured throughout the course of the microscopy experiments. The lateral resolution is approximately 4 µm with the employed setup. Simple image processing software is used to improve the contrast of the micrographs.
   1. Spread an aliquot of 100 µl of the dilute stock solution of (3) on ultrapure water in the Langmuir trough aligned with the Brewster angle microscope.
   2. Leave the Langmuir trough to equilibrate for 15 min, allowing the solvent to evaporate.
   3. Compress the layer to a surface pressure of 8 mN/m with a constant compression rate of 5 Å/(molecule x min) by reducing the surface area of the Langmuir trough with the barriers. Monitor the surface pressure by means of the surface pressure microbalance equipped with a filter paper Wilhelmy plate and set the barriers of the Langmuir trough so that a surface pressure of 8 mN/m is maintained.
   4. Record BAM micrographs at this surface pressure[46,47].

5. Carefully open the box enclosing the Langmuir trough. Mount the UV lamp to a support stand and place it approximately 50 cm away from the water surface while ensuring that the interface is covered in the cone of the UV light.
6. Make sure that the monolayer is still compressed at a surface pressure of 8 mN/m and fix the position of the barriers of the Langmuir trough.
7. Expose the air-water interface to UV light. Stop the irradiation by turning the lamp off after a total of 40 min. Monitor and record the change of the surface pressure throughout the course of the irradiation.
8. Record BAM micrographs after irradiation[46,47].
9. Use a needle to manipulate the carbon nanosheet at the air-water interface, and use the BAM to monitor the movement of the carbon nanosheet. Applying pressure to the carbon nanosheet leads to a rupture of the sheet.
10. Record BAM micrographs of the ruptured sheet[46,47].

3. Langmuir-Blodgett Transfer of an Uncarbonized Layer and a Carbon Nanosheet from the Air-water Interface to a Solid Substrate
Note: The sapphire (Al_2O_3) substrates are cleaned prior to transfer by a basic piranha treatment and stored in ultrapure water prior to use[48]. A pair of tweezers attached to a mechanical arm is placed vertically above a Langmuir trough with an appropriately deep cavity for the Langmuir-Blodgett (LB) transfer of layers from the air-water interface[49]. If the transfer of a non-carbonized as well as a carbonized sample is intended within the same experiment, as described here, two pairs of tweezers need to be attached to the mechanical arm at different heights so that one substrate can be removed while the second substrate remains immersed in the subphase. The Langmuir-Schäfer (LS) transfer was carried out manually with holey carbon transmission electron microscopy (TEM) grids as a support[50].
    1. Install two sapphire substrates with the two pairs of tweezers, immerse the substrates in the subphase, and thoroughly clean the air-water interface before spreading.
    2. Carefully spread an aliquot of 100 µl of the dilute stock solution of (3) in DCM/chloroform on ultrapure water in the Langmuir trough.
    3. Leave the Langmuir trough to equilibrate for 15 min allowing the solvent to evaporate.
    4. Compress the layer to a surface pressure of 8 mN/m with a constant compression rate of 5 Å/(molecule x min) by reducing the surface area of the Langmuir trough with the barriers. Monitor the surface pressure by means of the surface pressure microbalance equipped with a filter paper Wilhelmy plate and set the barriers of the Langmuir trough so that a surface pressure of 8 mN/m is maintained.
    5. In order to transfer the non-carbonized monolayer to a sapphire substrate, maintain the monolayer at a surface pressure of 8 mN/m as indicated by the surface pressure microbalance and pull the mechanical arm up at a speed of 1.2 mm/min until the first substrate is completely removed from the subphase. The second substrate needs to remain immersed in the subphase.
    6. Carefully retrieve the first substrate carrying the non-carbonized layer from the pair of tweezers, store it under protection from light and employ it for the intended application when needed.
    7. Carefully open the box enclosing the Langmuir trough. Mount the UV lamp to a support stand and place it approximately 50 cm away from the water surface, while ensuring that the interface is covered in the cone of the UV light.
    8. Ensure that the monolayer is still compressed at a surface pressure of 8 mN/m and fix the position of the barriers.
    9. Expose the air-water interface to UV light. Stop the irradiation by turning the lamp off after a total of 40 min of irradiation. Monitor and record the change of the surface pressure as measured by the surface pressure microbalance throughout the course of the irradiation.
    10. In order to transfer the carbonized film to a sapphire substrate, set the barriers of the Langmuir trough so that the surface pressure measured after irradiation is maintained. While keeping the surface pressure constant by the barriers of the Langmuir trough, retract the mechanical arm holding the substrate from the interface at a speed of 1.2 mm/min until the substrate is completely removed from the subphase.
    11. Carefully retrieve the substrate carrying the carbonized layer from the pair of tweezers.
    12. Hold a holey carbon TEM grid with a pair of tweezers and perform a manual LS transfer of the carbonized layer from the air-water interface[50]. Let the sample slowly dry in a gentle stream of nitrogen and perform scanning electron microscopy (SEM) imaging.
    13. Record UV/Vis absorption spectra of the non-carbonized layer and the carbon nanosheet on a UV/Vis spectrometer at a scan speed of 400 nm per minute. Use an empty sapphire substrate as the reference.

Representative Results

The ^{13}C nuclear magnetic resonance (NMR) spectrum of the prepared precursor molecule **3** displays the 12 *sp*-hybridized carbon atoms of the hexayne segment with the corresponding chemical shifts of δ = 82-60 ppm (**Figure 1b**). Moreover, the signals at δ = 173 ppm and at δ = 52 ppm are assigned to the carbonyl and methyl carbon of the ester, respectively. The signals between δ = 33-14 ppm are ascribed to the aliphatic carbons of the dodecyl residue. The corresponding UV/Vis absorption spectrum of **3** shows the characteristic vibronic fine structure of a hexayne (**Figure 1c**).

The film-forming properties of the hexayne amphiphile (3) are investigated by measurement of the surface pressure-area isotherm and by deriving the compressibility moduli (**Figure 2a-b**). Compression of the layer leads to an increase of the surface pressure at a mean molecular area of 24 $Å^2$ and the isotherm features a steep slope. Moreover, a strongly tilted plateau region is observed between surface pressures of 9 and 15 mN/m, corresponding to mean molecular areas of 22 and 18 $Å^2$, respectively. Above the plateau, a second steep increase of the slope of the isotherm is observed up to the collapse of the film at a surface pressure of 37 mN/m corresponding to a mean molecular area of 17 $Å^2$. A plot of the compressibility modulus versus the surface pressure shows that the former increases to values of C_s^{-1} >100 mN/m even at surface pressures as low as 1-9 mN/m. This is followed by a decrease of the modulus in the plateau region, and a further increase beyond values of C_s^{-1} >300 mN/m up to the collapse of the film. Monitoring the layer of (3) at a surface pressure of 8 mN/m shows no change in the corresponding surface area (**Figure 2c**). At a surface pressure of 23 mN/m above the plateau in the isotherm, however, a significant reduction of the surface area occurs over the course of 45 min (**Figure 2d**).

The self-assembled monolayer at surface pressures below the plateau in the isotherm is characterized by recording infrared reflection absorption (IRRA) spectra (**Figure 3**). The IRRA spectra at surface pressures of 1-8 mN/m show broad bands at 3,600 and 1,670 cm^{-1} that arise from the OH stretching and bending vibrations of water, respectively. Moreover, a band at 2,350 cm^{-1} is observed that originates from an insufficient compensation of the carbon dioxide signal (**Figure 3a**). Next to these background signals, the spectra display bands at 2,919 and 2,849 cm^{-1} corresponding to the asymmetric and symmetric CH_2 stretching vibrations of the dodecyl residues of amphiphile (3) (**Figure 3b**). The positions of these bands serve as qualitative markers for the conformational order of alkyl residues in monolayers at the air-water interface[45,51]. Moreover, bands at 2,200 and 2,171 cm^{-1} are observed that can be assigned to the C≡C stretching vibrations of the hexayne moiety (**Figure 3c**). The IRRA spectra do not change upon compression of the layer to different surface pressures below the plateau in the isotherm.

The carbonization process is monitored by IRRA spectroscopy and the evolution of the surface pressure is followed by means of the surface pressure microbalance (**Figure 4**). A comparison of the IRRA spectra before and after UV irradiation shows that the vibrational band associated with the hexayne moieties (ν(C≡C)) at 2,200 and 2,172 cm^{-1} has completely disappeared after 40 min of irradiation (**Figure 4c**). At the same time, the asymmetric and symmetric methylene stretching vibrations at 2,919 and 2,849 cm^{-1} decrease in intensity and shift to frequencies of 2,924 and 2,855 cm^{-1}, respectively (**Figure 4b**). Moreover, the OH band of the subphase (ν(OH)) at 3,600 cm^{-1} significantly decreases in intensity in the course of irradiation (**Figure 4a**). The data from the surface pressure microbalance show that, when the barriers are fixed after compression of the monolayer to 8 mN/m and the UV irradiation is started, the surface pressure rapidly increases beyond values of 27 mN/m in the course of the carbonization process.

Films transferred to sapphire substrates after the UV-induced carbonization show a broad, featureless absorption at wavelengths of up to 550 nm in the respective UV/Vis spectrum (**Figure 4e**). The main absorption peak of the carbon nanosheets is observed at approximately 260 nm, and the comparison with the spectrum of the monolayer before irradiation confirms the complete conversion of the hexayne moieties. Brewster angle micrographs (**Figure 5**) and scanning electron microscopy (SEM) images serve as a means to visualize the obtained carbon nanosheets (**Figure 6**). While Brewster angle micrographs of a monolayer of the amphiphile (3) compressed to 8 mN/m show a film with imperfections or voids as indicated by the black regions (**Figure 5a**), the images of the layer obtained after carbonization by UV irradiation display a distinct change in the texture of the film (**Figure 5b, c**). After rupture of the sheet islands remain floating at the air-water interface (**Figure 5d**). Electron microscopy shows nanosheets after Langmuir-Schäfer transfer to a holey carbon TEM grid as support. The nanosheets are mechanically stable enough to span the micrometer-sized holes in a TEM grid (**Figure 6a-d**). A slight contrast is observed between regions covered with the carbon nanosheet and others at an accelerating voltage of 2.0 kV (**Figure 6a**; the dark spot visible in the image arises from the small working distance leading to a shadowing effect at low magnifications). Images taken at the same position highlight the influence of the accelerating voltage, as the carbon nanosheet becomes opaque to the electron beam at around 0.5 kV, and the carbon nanosheet shows draping as well as wrinkles at its edge (**Figure 6b, c**). The film is otherwise very smooth and uniformly spread over the grid further away from the border region (**Figure 6d**; the defect in the supporting grid aids in identifying the carbon nanosheet).

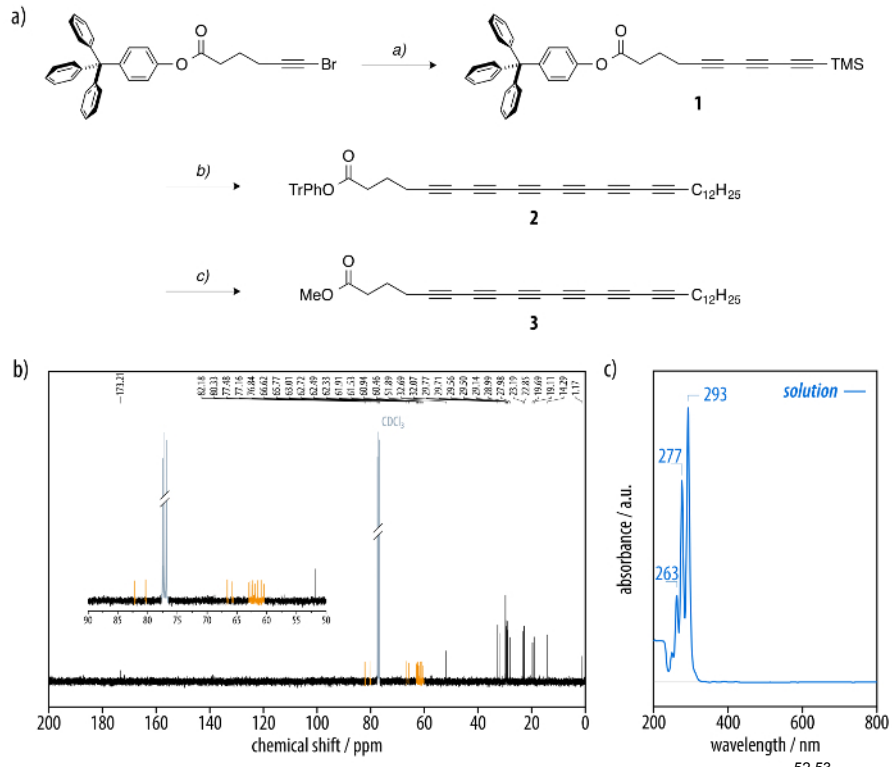

Figure 1: (**a**) Synthesis of the hexayne amphiphile (3) by the sequential bromination[52,53] and Pd-catalyzed elongation[30,31] of the alkyne segment. Reagents and conditions: (i) 1,4-bis(trimethylsilyl)buta-1,3-diyne, MeLi · LiBr, $ZnCl_2$, $PdCl_2$(dppf) · DCM, THF/toluene, 71%; ii) AgF, NBS, MeCN; then 1-trimethylsilyloctadeca-1,3,5-triyne **7**, MeLi · LiBr, $ZnCl_2$, $PdCl_2$(dppf) · DCM, THF/toluene, 23% over two steps; (iii) NaOMe, DCM, MeOH, quantitative. (**b**) The ^{13}C NMR spectrum of the hexayne amphiphile (3) with twelve acetylene carbon resonances (orange) and (**c**) the corresponding UV/Vis spectrum. Please click here to view a larger version of this figure.

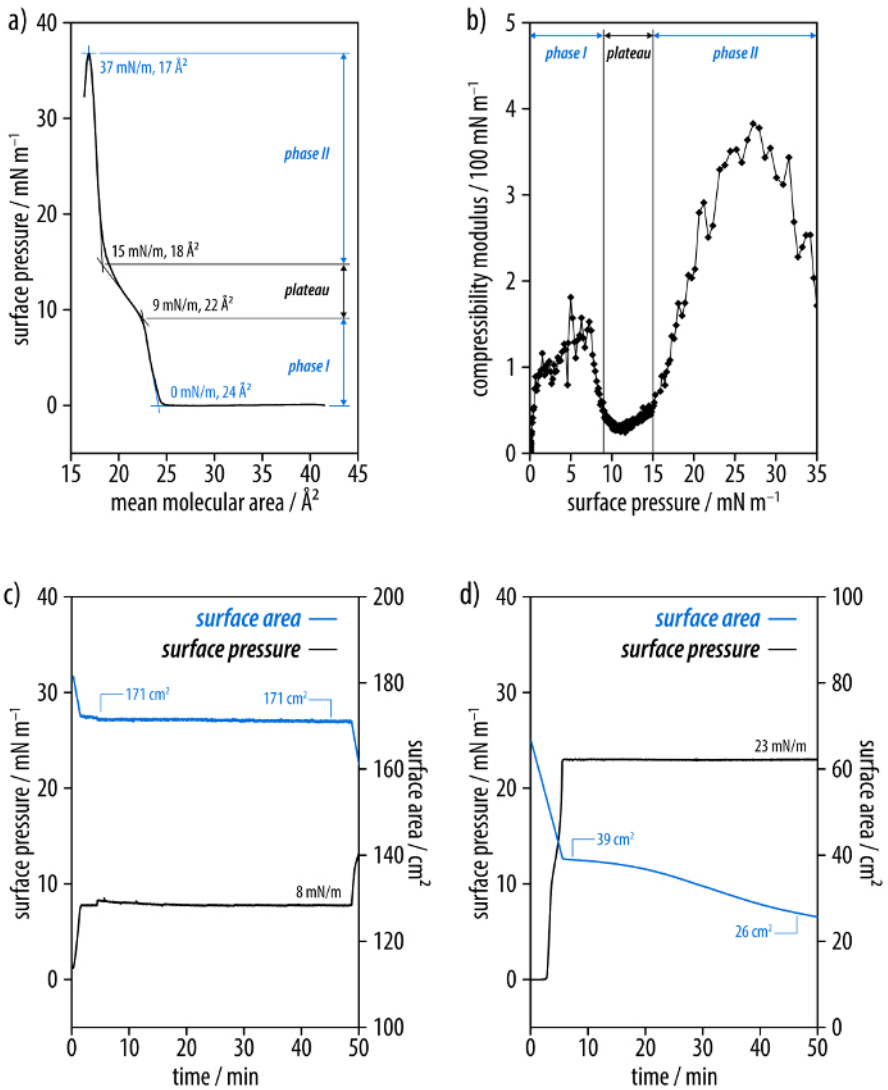

Figure 2: Investigation of the hexayne amphiphile (3) at the air-water interface. (**a**) The surface pressure area isotherm and (**b**) the plot of the compressibility modulus of the film indicate a direct transition from a gas-analogous phase to a condensed phase. (**c**) A layer is compressed to 8 mN/m as well as (**d**) 23 mN/m, and the development of the surface area is monitored at constant surface pressure. Please click here to view a larger version of this figure.

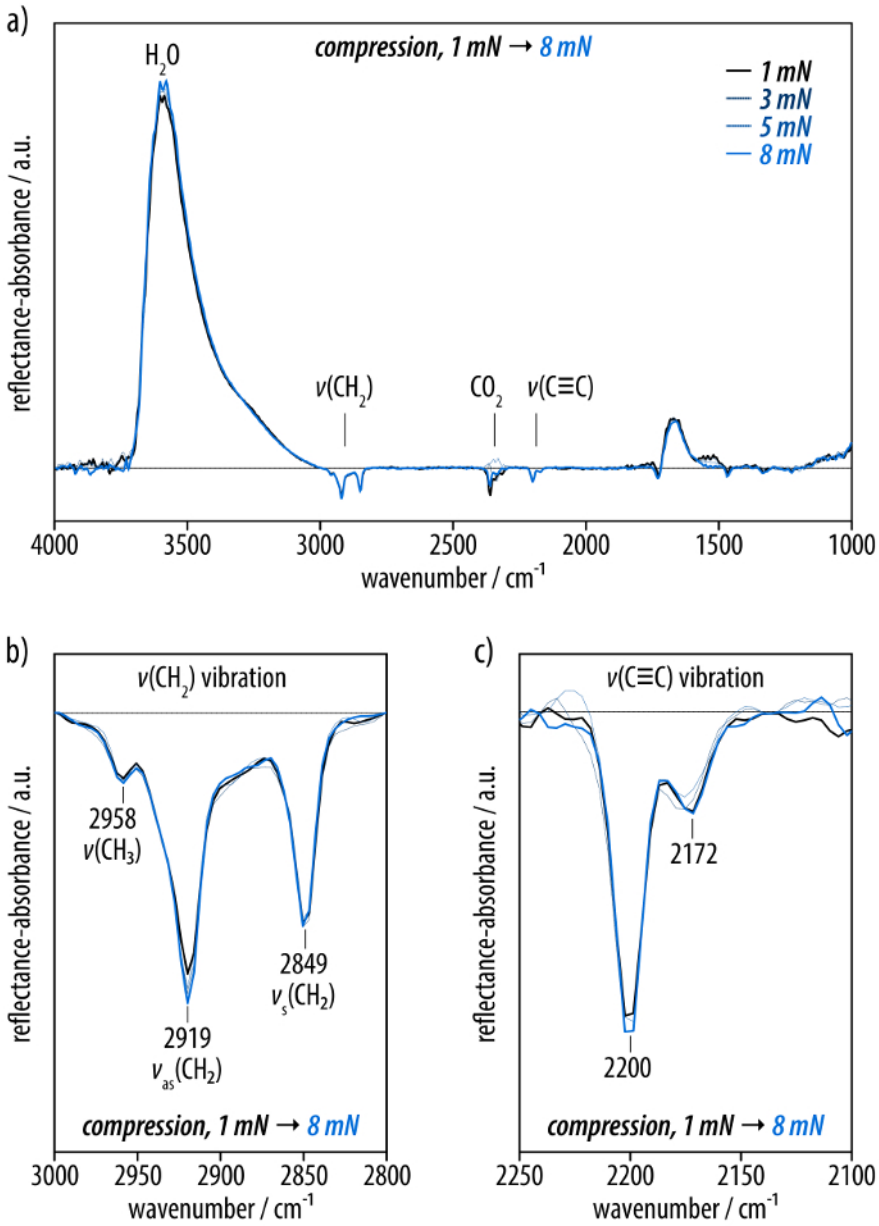

Figure 3: Infrared reflection-absorption (IRRA) spectra of the film of the hexayne amphiphile (3) (40°, *p*-polarized light) compressed to surface pressures between 1 mN/m (black line) and 8 mN/m (light blue line). (**a**) The full spectrum with prominent bands at 3,600 and 1,670 cm^{-1} from the water subphase as well as the peak around 2,350 cm^{-1} due to insufficient carbon dioxide compensation. (**b**) The spectral region of the methylene stretching vibrations as well as (**c**) the bands corresponding to the hexayne moiety. Please click here to view a larger version of this figure.

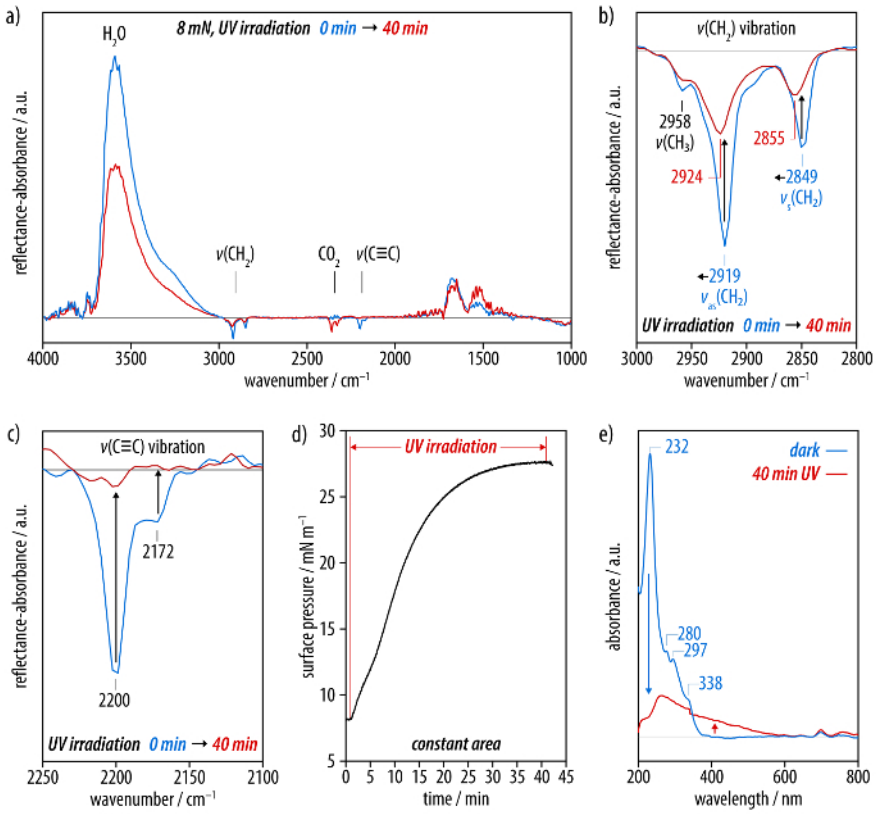

Figure 4: Investigation of the carbonization of a film of the reactive, carbon-rich amphiphile 3. (**a**) IRRA spectra recorded before (blue line) and after 40 min (red line) of UV irradiation. (**b**) The spectral region of the methylene stretching vibrations as well as (**c**) the bands corresponding to the hexayne moiety. (**d**) With the barriers fixed to a constant surface area, a significant increase in the surface pressure is observed during the carbonization. (e) UV/Vis spectra of irradiated films in comparison to a non-carbonized film of (3) show a broad and featureless absorption at wavelengths of up to 600 nm. Please click here to view a larger version of this figure.

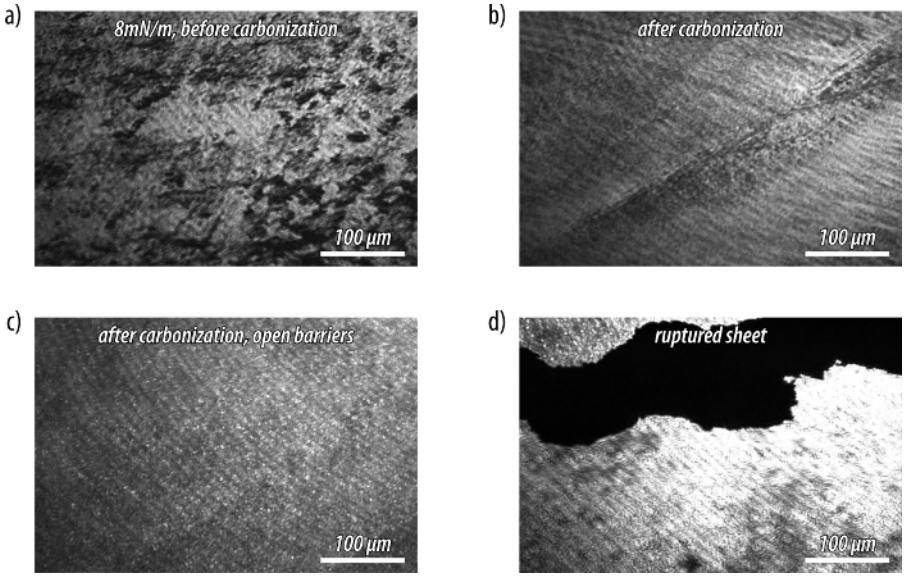

Figure 5: Brewster angle microscopy (BAM) experiments with a film of amphiphile 3 at the air-water interface before and after carbonization by UV irradiation. (**a**) Micrograph of a monolayer of (3) compressed to 8 mN/m. (**b**) After UV irradiation, a clear change in the texture of the film is observed that (**c**) becomes more homogenous after allowing the film to expand by opening the barriers. (**d**) Rupture of the carbonized sheet by manipulation with a needle leaves islands floating at the air-water interface. Please click here to view a larger version of this figure.

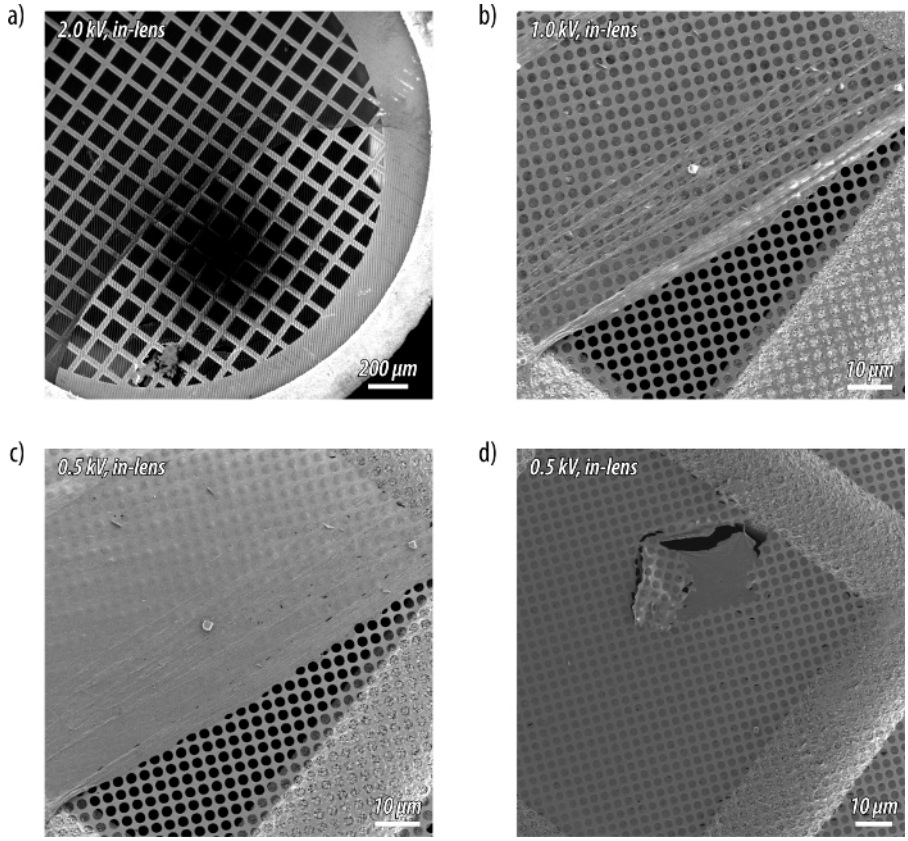

Figure 6: Scanning electron microscopy (SEM) of a carbon nanosheet after Langmuir-Schäfer transfer to a holey carbon TEM grid as support. (**a**) A partially covered grid imaged at an accelerating voltage of 2.0 kV. (**b**-**c**) The carbon nanosheet becomes opaque to the electron beam at around 0.5 kV. (**d**) Away from the edge, a smooth film uniformly spreads the grid. Please click here to view a larger version of this figure.

Discussion

The desired hexayne amphiphile (3) is straightforwardly prepared by the sequential bromination[52,53] and Pd-catalyzed elongation[30,31] of the alkyne segment, followed by a final deprotection reaction of the tritylphenyl ester (2) (**Figure 1a**)[29]. The successful synthesis is confirmed by the ^{13}C NMR spectrum (**Figure 1b**) as well as the UV-Vis absorption spectrum (**Figure 1c**)[31,54]. This demonstrates the facile nature by which higher oligoyne homologues can be prepared by the developed synthetic methodology[30,31]. However, it is important to keep the sensitivity of oligoyne derivatives in mind, and their storage in dilute solutions is advisable in order to ensure long-term integrity. Moreover, neat compounds should be handled in the dark at or below room temperature to avoid any premature decomposition. This is of critical importance for the bromotriyne intermediate that is prepared *in situ* in the synthesis of the hexayne ester (2), as this compound readily dimerizes in the solid state[41]. The hexayne amphiphile (3) reversibly forms films at the air-water interface (**Figure 2a, b**), undergoing successive transitions from a gas-analogous phase to two different condensed phases separated by a plateau[55]. Monitoring the development of the surface area over time at a constant surface pressure proved that the films were stable at pressures below the plateau (**Figure 2c, d**). The carbonization of the monolayer was therefore investigated at a surface pressure of 8 mN/m. In order to achieve reproducible measurements of the surface pressure area isotherm, a clean Langmuir trough setup is of utmost importance.

IRRA spectra display bands for the asymmetric and symmetric methylene stretching vibrations at 2,919 and 2,849 cm^{-1}, characteristic for alkyl groups in a condensed and ordered *all-trans* state (**Figure 3a, b**)[45,51]. The bands at 2,200 and 2,171 cm^{-1} can be assigned to the C≡C stretching vibrations of the hexayne moiety (**Figure 3c**). Upon UV irradiation of the self-assembled monolayer, these bands completely disappear, indicating a virtually complete conversion (**Figure 4a-c**). The methylene stretching vibrations shift to frequencies of 2,924 and 2,855 cm^{-1} (**Figure 4b**), indicating that the dodecyl chains undergo a conformational change to a liquid-expanded, unordered (*gauche*) state[45,51]. A significant increase of the surface pressure occurs throughout the carbonization at a constant surface area, suggesting a lateral expansion of the layer upon carbonization (**Figure 4d**). Monolayers before and after carbonization are then transferred to sapphire substrates. Different from the hexayne (3) in solution and the non-irradiated monolayer, the UV/Vis spectrum of the carbonized film showed a broad, featureless absorption at wavelengths of up to 550 nm, providing conclusive evidence of the extensive carbonization (**Figure 4e**). The optical band gap of approximately 2.2 eV thus suggests the presence of at least nanometer-sized domains of graphitic carbon, according to studies of reduced graphene oxide materials[56,57].

Brewster angle micrographs of a monolayer of the amphiphile (3) before carbonization show a film with imperfections or voids as indicated by the black regions (**Figure 5a**). By contrast, images of the monolayer after carbonization display a more homogeneous film with a corrugated texture (**Figure 5b**), even after expansion of the barriers of the Langmuir trough (**Figure 5c**). The carbonized films can be ruptured by manipulation with a needle, and the ruptured islands remain floating at the air-water interface (**Figure 5d**). This corroborates the drastically increased mechanical

stability of the films after carbonization. Moreover, SEM micrographs confirm the formation of a thin carbon nanosheet with extended lateral dimensions (**Figure 6a-d**).

In conclusion, we have herein presented a new method to prepare carbon nanosheets based on the self-assembly and subsequent carbonization of amphiphilic hexaynes at the air-water interface. This process yields mechanically stable functionalized carbon films that bear similarities to reduced graphene oxide in their carbon structure. The lateral dimensions of the carbon nanosheets are only limited by the area of the Langmuir trough and square centimeter sized nanosheet samples are straightforwardly prepared. Notably, the presented approach achieves a complete carbonization at room temperature, which distinguishes it significantly from other approaches toward carbon nanomaterials that typically rely on process temperatures above 800 °C[18,58,59]. Accordingly, chemical functional groups are retained and a control of the surface chemistry of the carbon nanosheets can be achieved through a careful choice of the amphiphilic precursor molecules. We foresee a plethora of potential applications from the preparation of chemoselective substrates for electron-microscopy to protective coatings, novel electrode materials, and membranes.

Disclosures

The authors have nothing to disclose.

Acknowledgements

Funding from the European Research Council (ERC Grant 239831) and a Humboldt Fellowship (BS) is gratefully acknowledged.

References

1. Geim, A. K., & Novoselov, K. S. The rise of graphene. *Nature Mater.* **6** (3), 183-191 (2007).
2. Lee, C., Wei, X., Kysar, J. W., & Hone, J. Measurement of the Elastic Properties and Intrinsic Strength of Monolayer Graphene. *Science.* **321** (5887), 385-388 (2008).
3. Lee, J.-H., Loya, P. E., Lou, J., & Thomas, E. L. Dynamic mechanical behavior of multilayer graphene via supersonic projectile penetration. *Science.* **346** (6213), 1092-1096 (2014).
4. Castro Neto, A. H., Guinea, F., Peres, N. M. R., Novoselov, K. S., & Geim, A. K. The electronic properties of graphene. *Rev. Mod. Phys.* **81** (1), 109-162 (2009).
5. Lau, C. N., Bao, W., & Velasco, J., Jr Properties of suspended graphene membranes. *Mater. Today*. **15** (6), 238-245 (2012).
6. Ramanathan, T. *et al.* Functionalized graphene sheets for polymer nanocomposites. *Nature Nanotechnol.* **3** (6), 327-331 (2008).
7. Fan, Z., Yan, J., Ning, G., Wei, T., Zhi, L., & Wei, F. Porous graphene networks as high performance anode materials for lithium ion batteries. *Carbon.* **60**, 558-561 (2013).
8. Fiori, G. *et al.* Electronics based on two-dimensional materials. *Nature Nanotechnol.* **9** (10), 768-779 (2014).
9. Burghard, M., Klauk, H., & Kern, K. Carbon-Based Field-Effect Transistors for Nanoelectronics. *Adv. Mater.* **21** (25-26), 2586-2600 (2009).
10. Avouris, P., Chen, Z., & Perebeinos, V. Carbon-based electronics. *Nature Nanotechnol.* **2** (10), 605-615 (2007).
11. Zurutuza, A., & Marinelli, C. Challenges and opportunities in graphene commercialization. *Nature Nanotechnol.* **9** (10), 730-734 (2014).
12. Novoselov, K. S., Fal'ko, V. I., Colombo, L., Gellert, P. R., Schwab, M. G., & Kim, K. A roadmap for graphene. *Nature*. **490** (7419), 192-200 (2013).
13. Novoselov, K. S. *et al.* Electric field effect in atomically thin carbon films. *Science* **306** (5696), 666-669 (2004).
14. Li, X. *et al.* Large-Area Synthesis of High-Quality and Uniform Graphene Films on Copper Foils. *Science* **324** (5932), 1312-1314 (2009).
15. Sun, Z., Yan, Z., Yao, J., Beitler, E., Zhu, Y., & Tour, J. M. Growth of graphene from solid carbon sources. *Nature.* **468** (7323), 549-552 (2010).
16. Lee, J.-H. *et al.* Wafer-scale growth of single-crystal monolayer graphene on reusable hydrogen-terminated germanium. *Science*. **344** (6181), 286-289 (2014).
17. Scott, L. T. *et al.* A rational chemical synthesis of C60. *Science* **295** (5559), 1500-1503 (2002).
18. Hoheisel, T. N., Schrettl, S., Szilluweit, R., & Frauenrath, H. Nanostructured Carbonaceous Materials from Molecular Precursors. *Angew. Chem. Int. Ed.* **49** (37), 6496-6515 (2010).
19. Schrettl, S., & Frauenrath, H. Elements for a Rational Polymer Approach towards Carbon Nanostructures. *Angew. Chem. Int. Ed.* **51** (27), 6569-6571 (2012).
20. Müllen, K. Evolution of Graphene Molecules: Structural and Functional Complexity as Driving Forces behind Nanoscience. *ACS Nano.* **8** (7), 6531-6541 (2014).
21. Chen, L., Hernandez, Y., Feng, X., & Müllen, K. From Nanographene and Graphene Nanoribbons to Graphene Sheets: Chemical Synthesis. *Angew. Chem. Int. Ed.* **51** (31), 7640-7654 (2012).
22. Paraknowitsch, J. P., & Thomas, A. Functional Carbon Materials From Ionic Liquid Precursors. *Macromol. Chem. Phys.* **213** (10-11), 1132-1145 (2012).
23. Titirici, M.-M. *et al.* Sustainable carbon materials. *Chem. Soc. Rev.* **44** (1), 250-290 (2015).
24. Angelova, P. *et al.* A universal scheme to convert aromatic molecular monolayers into functional carbon nanomembranes. *ACS Nano* **7** (8), 6489-6497 (2013).
25. Zhi, L., Wu, J., Li, J., Kolb, U., & Müllen, K. Carbonization of Disclike Molecules in Porous Alumina Membranes : Toward Carbon Nanotubes with Controlled Graphene-Layer Orientation. *Angew. Chem. Int. Ed.* **44** (14), 2120-2123 (2005).
26. Zhi, L. *et al.* From Well-Defined Carbon-Rich Precursors to Monodisperse Carbon Particles with Hierarchic Structures. *Adv. Mater.* **19** (14), 1849-1853 (2007).
27. Matei, D. G. *et al.* Functional single-layer graphene sheets from aromatic monolayers. *Adv. Mater.* **25** (30), 4146-4151 (2013).
28. Szilluweit, R. *et al.* Low-temperature preparation of tailored carbon nanostructures in water. *Nano Lett.* **12** (5), 2573-2578 (2012).
29. Schrettl, S. *et al.* Functional carbon nanosheets prepared from hexayne amphiphile monolayers at room temperature. *Nature Chem.* **6** (6), 468-476 (2014).

30. Hoheisel, T. N., & Frauenrath, H. A Convenient Negishi Protocol for the Synthesis of Glycosylated Oligo(ethynylene)s. *Org. Lett.* **10** (20), 4525-4528 (2008).
31. Schrettl, S. *et al.* Facile synthesis of oligoyne amphiphiles and their rotaxanes. *Chem. Sci.* **6** (1), 564-574 (2015).
32. Sakamoto, J., van Heijst, J., Lukin, O., & Schlüter, A. D. Two-Dimensional Polymers: Just a Dream of Synthetic Chemists? *Angew. Chem. Int. Ed.* **48** (6), 1030-1069 (2009).
33. Bauer, T. *et al.* Synthesis of Free-Standing, Monolayered Organometallic Sheets at the Air/Water Interface. *Angew. Chem. Int. Ed.* **50** (34), 7879-7884 (2011).
34. Payamyar, P. *et al.* Synthesis of a Covalent Monolayer Sheet by Photochemical Anthracene Dimerization at the Air/Water Interface and its Mechanical Characterization by AFM Indentation. *Adv. Mater.* **26** (13), 2052-2058 (2014).
35. Zheng, Z. *et al.* Synthesis of Two-Dimensional Analogues of Copolymers by Site-to-Site Transmetalation of Organometallic Monolayer Sheets. *J. Am. Chem. Soc.* **136** (16), 6103-6110 (2014).
36. Sakamoto, R. *et al.* A photofunctional bottom-up bis(dipyrrinato)zinc(II) complex nanosheet. *Nature Commun.* **6**, 6713 (2015).
37. van Heijst, J., Corda, M., & Lukin, O. Compounds bearing multiple photoreactive chalcone units: Synthesis and study towards 2D polymerization in Langmuir monolayers. *Polymer.* **70**, 1-7 (2015).
38. Murray, D. J. *et al.* Large area synthesis of a nanoporous two-dimensional polymer at the air/water interface. *J. Am. Chem. Soc.* **137** (10), 3450-3453 (2015).
39. Li, J. J., Limberakis, C., & Pflum, D. A. *Modern Organic Synthesis in the Laboratory.* Oxford University Press: New York, NY, USA, (2007).
40. Chai, C., & Armarego, W. L. F. *Purification of Laboratory Chemicals.* Elsevier Butterworth-Heinemann: Burlington, MA, USA, (2003).
41. Hoheisel, T. N. *et al.* A multistep single-crystal-to-single-crystal bromodiacetylene dimerization. *Nature Chem.* **5** (4), 327-334 (2013).
42. Brzozowska, A. M., Duits, M. H. G., & Mugele, F. Stability of stearic acid monolayers on Artificial Sea Water. *Colloids Surf., A.* **407**, 38-48 (2012).
43. Davies, J. T., & Rideal, E. K. *Interfacial Phenomena.* Academic Press: New York, NY, USA, (1963).
44. Mendelsohn, R., & Flach, C. R. Infrared Reflection-Absorption Spectrometry of Monolayer Films at the Air-Water Interface. *Handbook of Vibrational Spectroscopy.* 1028-1041 J. Wiley & Sons: Chichester, UK, (2002).
45. Mendelsohn, R., Mao, G., & Flach, C. R. Infrared reflection-absorption spectroscopy: Principles and applications to lipid-protein interaction in Langmuir films. *Biochim. Biophys. Acta Biomembr.* **1798** (4), 788-800 (2010).
46. Hoenig, D., & Moebius, D. Direct visualization of monolayers at the air-water interface by Brewster angle microscopy. *J. Phys. Chem.* **95** (12), 4590-4592 (1991).
47. Hénon, S., & Meunier, J. Microscope at the Brewster angle: Direct observation of first-order phase transitions in monolayers. *Rev. Sci. Instrum.* **62** (4), 936-939 (1991).
48. Kirby, K. W., Shanmugasundaram, K., Bojan, V., & Ruzyllo, J. Interactions of Sapphire Surfaces with Standard Cleaning Solutions. *ECS Trans.* **11** (2), 343-349 (2007).
49. Blodgett, K. B. Films Built by Depositing Successive Monomolecular Layers on a Solid Surface. *J. Am. Chem. Soc.* **57** (6), 1007-1022 (1935).
50. Langmuir, I., & Schaefer, V. J. Activities of Urease and Pepsin Monolayers. *J. Am. Chem. Soc.* **60** (6), 1351-1360 (1938).
51. Mendelsohn, R., Brauner, J. W., & Gericke, A. External infrared reflection absorption spectrometry of monolayer films at the air-water interface. *Annu. Rev. Phys. Chem.* **46** (1), 305-334 (1995).
52. Hofmeister, H., Annen, K., Laurent, H., & Wiechert, R. A Novel Entry to 17a-Bromo- and 17a-Iodoethynyl Steroids. *Angew. Chem. Int. Ed. Engl.* **23** (9), 727-729 (1984).
53. Kim, S., Kim, S., Lee, T., Ko, H., & Kim, D. A New, Iterative Strategy for the Synthesis of Unsymmetrical Polyynes: Application to the Total Synthesis of 15,16-Dihydrominquartynoic Acid. *Org. Lett.* **6** (20), 3601-3604 (2004).
54. Chalifoux, W. A., & Tykwinski, R. R. Synthesis of polyynes to model the sp-carbon allotrope carbyne. *Nature Chem.* **2** (11), 967-971 (2010).
55. Kaganer, V. M., Möhwald, H., & Dutta, P. Structure and phase transitions in Langmuir monolayers. *Rev. Mod. Phys.* **71** (3), 779-819 (1999).
56. Eda, G. *et al.* Blue photoluminescence from chemically derived graphene oxide. *Adv. Mater.* **22** (4), 505-509 (2010).
57. Kumar, P. V., Bardhan, N. M., Tongay, S., Wu, J., Belcher, A. M., & Grossman, J. C. Scalable enhancement of graphene oxide properties by thermally driven phase transformation. *Nature Chem.* **6** (2), 151-158 (2014).
58. Chernick, E. T., & Tykwinski, R. R. Carbon-rich nanostructures: the conversion of acetylenes into materials. *J. Phys. Org. Chem.* **26** (9), 742-749 (2013).
59. Rondeau-Gagné, S., & Morin, J.-F. Preparation of carbon nanomaterials from molecular precursors. *Chem. Soc. Rev.* **43** (1), 85-98 (2014).

